STRUCTURAL CONTROL AND HEALTH MONITORING
Struct. Control Health Monit. 2011; **18**:361–381
Published online 21 January 2010 in Wiley Online Library (wileyonlinelibrary.com). DOI: 10.1002/stc.374

Optimization of the power flow extracted from a flexible structure using a control approach

D. Mammosser*,†, E. Foltête and M. Collet

Institut FEMTO-ST—Département de Mécanique Appliquée UMR CNRS 6174, University of Franche-Comté, 24 Chemin de l'Epitaphe, 25000 Besançon, France

SUMMARY

Vibrating energy is a renewable energy that can be used to power wireless transducers. This article presents analytical and numerical results that put forward design parameters for optimizing the energy conversion from mechanical vibration to electrical power with an electromagnetic transducer. The studied structure is a flexible structure using an electromagnetic transducer connected to a resistive feedback loop. This passive harvesting circuit is a simplified representation of the storing system usually including a battery and a rectifying electronic. Here the energy harvesting strategy chosen creates an additional viscous damping on the structure. The numerical model of the generator, including the coupling law, predicts the power transferred between electrical and mechanical energies. For a purely resistive feedback, the study of the harvested energy shows that harvesting and stabilization strategies are different. A simple analytical model, derived from modal synthesis techniques, shows that Jacobi's maximal power transfer theorem can be adapted for multi-physic problems: the electrical and mechanical damping ratios have to be matched to maximize the power transferred. This result is confirmed by experimental measurements. The analytical study also shows that it is possible to use the root locus to choose the two optimal energy harvesting feedback gains and then consequently the harvesting electronic circuit's parameters. Copyright © 2010 John Wiley & Sons, Ltd.

Received 27 August 2009; Revised 20 October 2009; Accepted 6 November 2009

KEY WORDS: energy harvesting; flexible structure; viscous damping; electromagnetic transducer; finite power source; optimization; control strategy; direct velocity feedback

1. INTRODUCTION

Nowadays wasting energy is of increasing concern. There are a lot of different energy sources available around us: the sun, the wind, rivers,…, but most of theses energies cannot be used directly. They first have to be transformed into another energy. For example, mechanical energy from a wave is transformed into electrical energy by an electromagnetic device [1]. This transformation is performed as electrical energy is very easy to carry and use. This explains why most of today's appliances use electrical energy.

Portable appliances have to be energetically autonomous: that is why the energy is stored in batteries, which need to be replaced regularly. An alternative solution is to harvest the available wasted vibrating energy and to convert it into electrical energy. This power scavenged from

*Correspondence to: D. Mammosser, Institut FEMTO-ST—Département de Mécanique Appliquée UMR CNRS 6174, University of Franche-Comté, 24 Chemin de l'Epitaphe, 25000 Besançon, France.
†E-mail: didier.mammosser@univ-fcomte.fr

Contract/grant sponsor: Publishing Arts Research Council; contract/grant number: 98-1846389

a vibrating structure can be used to power sensors [2,3] and hence for monitoring applications [4–6]. Piezoelectric [7,8], electrostatic [9,10] and electromagnetic [11,12] transducers have already been used to harvest energy in this way. Comparisons between different types of transducer architecture [13–15] have shown that in some cases there is interest in using a velocity-damped resonant generator [13]. Therefore, this study will focus on an electromagnetic power generator that produces a damping force proportional to the structural velocity. A consequence of energy harvesting is an additional damping on the structure [16]. In many cases, the harvested energy is very low compared to the energy stored in the power source, so the additional damping can be neglected. The structure is then considered as an infinite power source and does not suffer any harvesting feedback effect. For designing human body energy harvesting systems this assumption is made [14]. The limb's motion is then not disturbed by the scavenged energy. Williams *et al.* [17] also consider an infinite power source and optimize the energy harvesting in the case of a magnetic seismic mass moving past a coil connected to a resistive load. Nevertheless, some applications may not satisfy this hypothesis of infinite power source, for example, when using a harvesting system on a light and flexible panel, which is a common structure in the aerospace and automotive fields. A finite power source must then be considered, like in Monnier *et al.* stabilization approach [18]. In this study the considered finite power source is a flexible structure, energetically supplied by an external power source such as environmental acceleration or vibration noise. To harvest energy one or more devices are connected to the flexible structure. The goal of this study is to maximize the power harvested from the structure with electromagnetic transducers.

The most realistic multi-physic modeling of the tested setup is written to study the influence of energy harvesting on the structure. The coupling electromechanical equations are added to the finite element model (FEM) of the flexible structure. This FEM is used to evaluate the energy provided by the external source and harvested by the studied transducer versus the resistive feedback, mimicking the effect of the harvesting electronics.

For frequencies close to a separated mode, the structure can be simplified by modal projection. The full coupled system can then be solved analytically and the influent parameters for optimizing energy harvesting can be carried out.

Section 2 presents the criterion to harvest energy. Section 3 compares the energy harvesting and the stabilization strategies. Section 4 models the flexible structure with the connected energy harvester. This modeling is used to evaluate the provided and harvested energies in Section 5. The modeling is simplified to obtain analytical expressions, which are compared to the numerical results. They are confirmed by experimental measurements presented in Section 6. Finally, in the last part of this paper, the conclusion presents the maximal power transfer condition for a viscous energy harvester and how to choose the corresponding feedback gain on the root locus.

2. HARVESTING ENERGY FROM A FLEXIBLE STRUCTURE

2.1. View from the flexible structure

Let us consider the vibrating structure shown in Figure 1.

The governing equation of the flexible structure is:

$$M_s\ddot{x}+C_s\dot{x}+K_sx = f \tag{1}$$

M_s, K_s, and C_s are respectively the mass, stiffness and damping symmetric matrices of the flexible structure. x represents the displacement vector and $\dot{x}$ represents differentiation of x with respect to time. The external excitation force is noted f. In Figure 1 only the force at point i is represented. The instantaneous power provided to the structure can be written as: $P = \dot{x}^{\mathrm{T}}.f = \sum_{i=1}^{n} \dot{x}_i^{\mathrm{T}}.f_i^{a/s} = \sum_{i=1}^{n} P_i$. If the instantaneous power P_i at point i is positive this indicates that power is provided to the structure. If P_i is negative, power is extracted from the structure. The goal of this study is to extract power with an actuator. If the condition $P_i<0$

DOI: 10.1002/stc

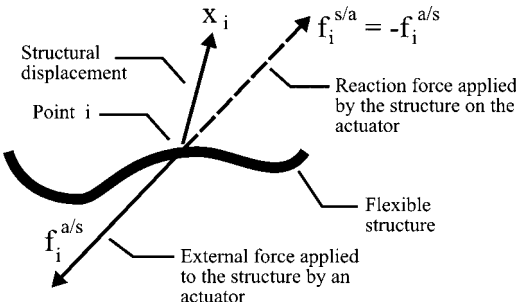

Figure 1. Extracting energy from a flexible structure.

(if $\dot{x}_i \neq 0$) is realized all the time energy is harvested. This strong condition implies $\int_0^\infty P_i \, dt$ negative. The condition $\int_{-\infty}^{\infty} P_i \, dt < 0$ is enough to consider that energy is harvested. By multiplying Equation (1) by $\dot{x}^T$ and integrating it, we obtain the following energy equation:

$$\left[\frac{1}{2}\dot{x}^T M_s \dot{x} + \frac{1}{2} x^T K_s x\right]_0^\infty + \int_0^\infty \dot{x}^T C_s \dot{x} \, dt = \int_0^\infty \dot{x}^T . f \, dt$$

$$= \sum_{i=1}^{p} \int_0^\infty \dot{x}_i^T . f_i^{a/s} \, dt + \sum_{i=p+1}^{n} \int_0^\infty \dot{x}_i^T . f_i^{a/s} \, dt \tag{2}$$

The points have been sorted such as the first p points provide energy to the structure, and the $n - p$ following ones harvest energy from it. $\int_{-\infty}^{\infty} \dot{x}_i^T . f_i^{a/s} \, dt \geqslant 0$ represents the energy provided at one of p first points and $\int_{-\infty}^{\infty} \dot{x}_i^T . f_i^{a/s} \, dt < 0$ the energy harvested at one of $n - p$ last ones. To harvest some energy the force $f_i^{a/s}$ has to be different from zero. This indicates that the energy harvesting device has to create a force on the structure.

2.2. View from the energy harvesting device

Figure 2 presents the energy harvesting device. x_i and x_j are the displacements imposed by the structure when the energy harvesting device is connected to the flexible structure. This is the configuration of the internal energy harvesting device shown in Figure 3. $f_i^{s/a}$ and $f_j^{s/a}$ are the reaction forces from the structure on the harvesting actuator.

We will assume that the transducer's mass is neglected compared to the forces $f_i^{s/a}$ and $f_j^{s/a}$. This implies that $f_j^{s/a} = -f_i^{s/a}$. The scavenged energy can then be written as:

$$E_{h_i} = \int_{-\infty}^{\infty} \dot{y}_i^T f_i^{s/a} \, dt = -\int_{-\infty}^{\infty} \dot{x}_i^T f_i^{a/s} \, dt - \int_{-\infty}^{\infty} \dot{x}_j^T f_j^{a/s} \, dt \tag{3}$$

This shows that an internal energy harvesting device extracts power from 2 points of the flexible structure. The power extracted from $n - p$ points of the flexible structure does not imply necessarily $n - p$ harvesting devices, unless we only consider external energy harvesting devices as shown in Figure 3. In this case the energy harvesting device is connected to one side of the flexible structure (displacement imposed to x_k) and the other side is fixed to the structure's support. The energy harvested by the device can be written as $E_{h_k} = \int_{-\infty}^{\infty} \dot{y}_k^T f_k^{s/a} \, dt$. In both cases the energy provided to the harvesting device is positive. For the rest of the study we will use the notation f_i for $f_i^{s/a}$. The harvesting criterion that we will use for an energy harvesting device i is:

$$E_{h_i} = \int_{-\infty}^{\infty} \dot{y}_i^T f_i \, dt > 0 \tag{4}$$

To maximize the scavenged energy, we will assume that the energy harvesting device, shown in Figure 2, is oriented such as the structure's force vector f_i is collinear to the velocity vector $\dot{y}_i$.

DOI: 10.1002/stc

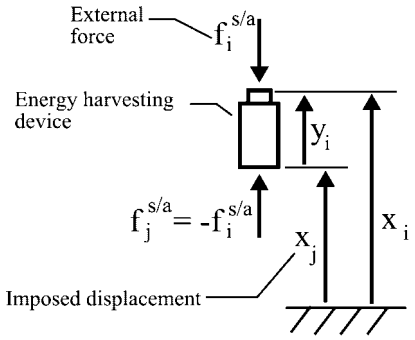

Figure 2. Modeling of an energy harvesting device.

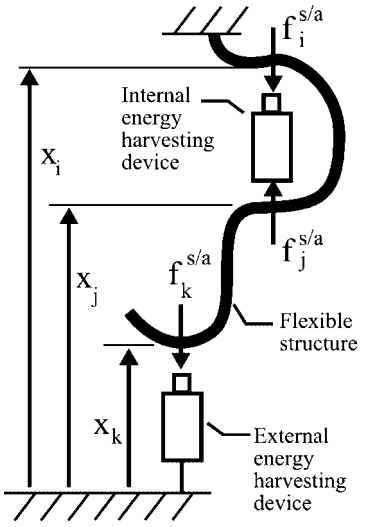

Figure 3. Energy harvesting devices connected to a flexible structure.

3. STABILIZATION VERSUS ENERGY HARVESTING STRATEGY

3.1. The direct velocity feedback control

To harvest energy from a flexible structure, a control law for f_i has to be defined. A simple solution is to suppose f_i proportional to the corresponding structural velocity $\dot{y}_i$.

$$f_i = g(\dot{y}_i) = g_i.\dot{y}_i \tag{5}$$

The control law is the simplest active damping strategy, and is commonly called direct velocity feedback (DVF). For a strictly positive gain g_i, the instantaneous power $g_i \dot{y}_i^{\mathrm{T}} \dot{y}_i$ is always positive, hence $E_{h_i} > 0$ if $\dot{y}_i \neq 0$. The governing equation of the flexible structure, for a DVF [19], is:

$$\begin{aligned} M_s\ddot{x} + C_s\dot{x} + K_s x &= f + Bu \\ \dot{y} &= B^{\mathrm{T}}\dot{x} \\ u &= -G \times \dot{y} \end{aligned} \tag{6}$$

$M_s > 0$, $K_s \geqslant 0$, and $C_s \geqslant 0$. The energy harvesting forces u apply a set of control forces Bu on the structure through the influence matrix B. The force vector u depends on the velocity measurements $\dot{y}$. As u and $\dot{y}$ are collocated, the same influence matrix B is used to evaluate $\dot{y}_i$. Hence, we have $\dot{y} = B^{\mathrm{T}}\dot{x}$. The external excitation force is noted as f. The power extracted from the vibrating structure corresponds to power harvested by the harvesting devices ($P_h = -\dot{y}^{\mathrm{T}}u$).

DOI: 10.1002/stc

According to Equation (6), the energy harvesting devices appear as an added mechanical dissipative impedance on the flexible structure. This has for effect to increase the structure's damping [16].

As the energy harvested depends on the additional structure's damping, optimizing the stabilization of the structure seems to be a good strategy. Are the energy harvesting and stabilization strategies really equivalent?

3.2. Stabilization strategy

To study the stability of the controlled system we have to find the complex roots of:

$$[M_s s^2+(C_s+\mathrm{BGB}^{\mathrm{T}})s+K_s]X=0 \tag{7}$$

This equation is obtained from Equation (6) and the system is always stable when $C_s+\mathrm{BGB}^{\mathrm{T}}>0$. The solutions of quadratic eigenvalue problem Equation (7) can then be written as [20]:

$$s_i=-\xi_i\omega_i \pm \mathrm{j}\omega_i\sqrt{1-\xi_i^2} \tag{8}$$

where $\omega_i \geqslant 0$ is the ith natural frequency and ξ_i the modal damping ratio of this mode. We will assume that $0 \leqslant \xi_i \leqslant 1$.

As $\Re(s_i) \leqslant 0$, the following inequality is verified:

$$|x_{(t)}| \leqslant \gamma \mathrm{e}^{\max[\Re e(s_i)]t} \tag{9}$$

where γ is a positive constant. Equation (9) corresponds to Komornik's result [21]. All the components are real positive values. Let us consider the fastest return of the structure to its equilibrium position as the stabilization strategy. This strategy is equivalent to minimize the cost function J_{st}:

$$J_{st\,(G)}=\max_{i\in[1;n]}\{\max[\Re(s_i)]\} \tag{10}$$

This criterion is equivalent to the one proposed by Monnier *et al.* [18], who optimize the stabilization of a flexible structure submitted to an integral force feedback (IFF). Meyer *et al.* [22] showed that the IFF optimization results are applicable to DVF strategy (as it is the dual form of IFF strategy). This explains why the IFF stabilization criterion can be applied as the harvesting devices impose a DVF control law.

From Equation (7) we can obtain the root locus in Figure 4. Only two modes (i and j) of the structure are represented. Each curve corresponds to the solution s of the mode i and j when the

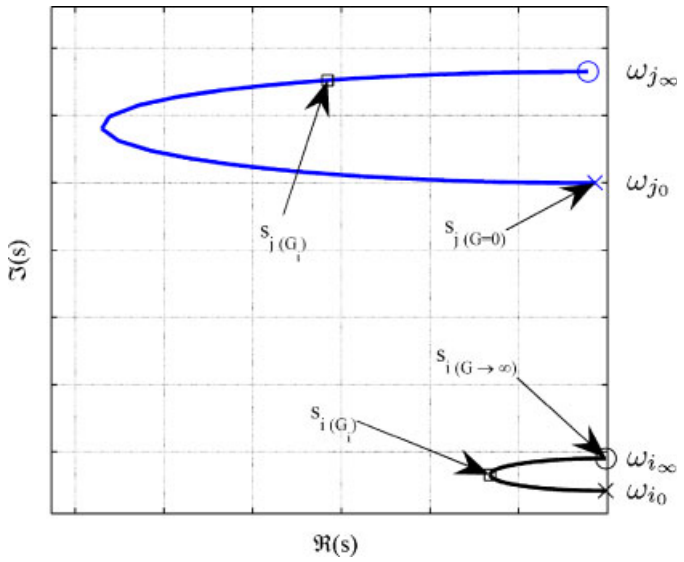

Figure 4. Example of root locus.

DOI: 10.1002/stc

feedback parameter G varies. In this figure, the solution $s_i(G_i)$ is marked. Here G_i minimizes $\Re(s_i(G))$. The cost function J_{st} defined only for the mode i is then minimized. This corresponds to the optimal damping feedback parameter for mode i.

In general, the optimal gain G_i does not optimize the stabilization of mode j, as it is shown in Figure 4. This means that each mode has its own optimal stabilization parameter G.

To optimize the stabilization of all the modes, the cost function has to be minimized considering all the modes. This means that the parameter G has to be chosen such as the highest solution $\Re(s(G))$ has to be minimal. If we consider the parameter G_i, it minimizes the shortest root locus loop (mode i). On the other curve we have $\Re(s_j(G_i)) < \Re(s_i(G_i))$, which means that for the two considered modes $J_{st}(G_i) \leqslant J_{st}(G)$. The stabilization is then optimized for $G = G_i$.

3.3. Energy harvesting strategy

The total energy harvested (E_h) from a flexible structure is:

$$E_h = \int_{-\infty}^{\infty} \dot{x}^{\mathrm{T}}(\mathrm{BGB}^{\mathrm{T}})\dot{x}\,\mathrm{d}t \tag{11}$$

When the matrix G is chosen positive, the harvested energy E_h is positive. If $f \in L^2_{\mathbb{R}}$, then we have $x \in L^2_{\mathbb{R}}$ and $E_h < \infty$ (Schwartz theorem). According to Parseval's theorem, it is possible to write the equality of energies between time and frequency domains:

$$E_h = \int_{-\infty}^{\infty} \dot{x}_{(t)}^{\mathrm{T}}(\mathrm{BGB}^{\mathrm{T}})\dot{x}_{(t)}, \quad \mathrm{d}t = \frac{1}{2\pi}\int_{-\infty}^{\infty} \dot{X}_{(-\mathrm{j}\omega)}^{\mathrm{T}}(\mathrm{BGB}^{\mathrm{T}})\dot{X}_{(\mathrm{j}\omega)}\,\mathrm{d}\omega \tag{12}$$

As $\dot{X} = \mathrm{j}\omega(-\omega^2 M_s + \mathrm{j}\omega(C_s + \mathrm{BGB}^{\mathrm{T}}) + K_s)^{-1}F$, this indicates that the maximal harvested energy (E_h) depends on G, f and ω. In the case of a periodic function f of period τ, it is not possible to use Equation (12) as $f \notin L^2_{\mathbb{R}}$ and then the energy harvested is not necessarily finite. But in the case $f \in L^2_{(\tau)}$, it is possible to give a new definition of the energy harvested (E_{h_τ}) on a time period.

$$E_{h_\tau} = \int_0^{\tau} \dot{x}^{\mathrm{T}}\left(\mathrm{BGB}^{\mathrm{T}}\right)\dot{x}\,\mathrm{d}t \tag{13}$$

We have $0 \leqslant E_{h_\tau} < \infty$. Maximizing the energy harvested is then equivalent to maximize the average power $P_h = E_{h_\tau}/\tau$ harvested on a time period. For a periodic function f, the Fourier's decomposition of $f_{(t)}$ and $\dot{x}_{(t)}$ gives:

$$\begin{aligned} f_{(t)} &= \sum_{n=-\infty}^{+\infty} f_n \mathrm{e}^{-\mathrm{j}n\omega t} \\ \dot{x}_{(t)} &= \sum_{n=-\infty}^{+\infty} (-\mathrm{j}n\omega).x_n \mathrm{e}^{-\mathrm{j}n\omega t} \end{aligned} \tag{14}$$

Let us note $\bar{x}_n$ the conjugated complex number of x_n. Applying Parseval's theorem to the real function $\dot{x}_{(t)}$ and noting that $\bar{\dot{x}}_n = \dot{x}_{-n}$, we obtain the relation:

$$\begin{aligned} P_h &= \frac{\omega}{2\pi}\int_0^{2\pi/\omega} \dot{x}_{(t)}^{\mathrm{T}}\left(\mathrm{BGB}^{\mathrm{T}}\right)\dot{x}_{(t)}\,\mathrm{d}t \\ &= \omega^2 \sum_{n=1}^{+\infty} n^2\, \bar{x}_n^{\mathrm{T}}\left(\mathrm{BGB}^{\mathrm{T}}\right) x_n \end{aligned} \tag{15}$$

As $x_n = (-n^2\omega^2 M_s + \mathrm{j}n\omega\,(C_s + \mathrm{BGB}^{\mathrm{T}}) + K_s)^{-1} f_n$, the average power harvested P_h depends on G, f, and ω. It is logical that the energy harvested depends on f as it imposes the incoming energy to the flexible structure.

From Equation (15) and x_n expression we can conclude that $P_{h\,(G=0)} = P_{h\,(G\to\infty)} = 0$. The average harvested power function versus G has then at least one maximum, as $P_{h\,(G)}$ is a continuous function and $P_h \geqslant 0$. Let us define the cost function J_h (for a periodic external applied force f to the structure):

$$J_{h\,(G,f,\omega)} = P_{h\,(G,f,\omega)} \tag{16}$$

DOI: 10.1002/stc

which has at least one maximum. In the case $f \in L_{(\mathbb{R})}^2$, similar results can be obtained by studying the total amount of energy harvested E_h instead of the average power for a periodic excitation f.

The cost function J_h can be used to decide if energy is harvested or not when G is not definite positive. In this case the inequality $J_h \geqslant 0$ has to be studied versus G.

3.4. Comparing energy harvesting and stabilization strategies

Energy harvesting and stabilization strategies are different as the definitions of the two cost functions J_{st} and J_h are not the same. In the case of stabilization, the defined cost function J_{st} depends only on the feedback loop parameter G. In the case of energy harvesting strategy, the cost function J_h depends on the same parameter G, the pulsation ω and the external force f. Does the parameter G_i which optimizes the stabilization of the mode i maximize the energy harvested?

The root locus can be used, as shown in Figure 4, to choose the optimal stabilization parameter G. We will prove in the energetic study Section 5 that the optimal stabilization parameter does not maximize the energy harvested in general. However, it will be shown that the root locus can still be used to choose the optimal energy harvesting parameter G when a viscous law control law is considered.

4. MODELING OF THE STRUCTURE WITH THE HARVESTING DEVICE

4.1. Modeling of the flexible structure without an energy harvesting device

If the considered flexible structure of Figure 3 is excited by an external harmonic force with pulsation close to one of its natural frequency, the structure can be modeled by a spring mass model.

Indeed, Equation (1) can be modified by considering the modal matrix (Φ) of the conservative system and the modal coordinate vector q_s, which satisfies the equation $x = \Phi q_s$. Operating Φ^{T} in Equation (1), the following equation is obtained:

$$\widetilde{M}_s \frac{\mathrm{d}^2 q_s}{\mathrm{d}t^2} + \widetilde{C}_s \frac{\mathrm{d}q_s}{\mathrm{d}t} + \widetilde{K}_s q_s = \Phi^{\mathrm{T}} f \tag{17}$$

with $M_s = \Phi^{\mathrm{T}} M_s \Phi = \mathrm{diag}(\mu_i)$, $K_s = \Phi^{\mathrm{T}} K_s \Phi = \mathrm{diag}(\mu_i \omega_i^2)$ and $\widetilde{C}_s = \Phi^{\mathrm{T}} C_s \Phi$. μ_i denotes the modal mass and ω_i the natural frequency of the mode i. Assuming a proportional damping model implies $\widetilde{C}_s = \mathrm{diag}(2\xi_i \omega_i \mu_i)$, where ξ_i is the modal damping ratio of the mode i. We will assume that $\xi_i 1$.

The Laplace transform of Equation (17) gives:

$$X = [\Phi(s^2 \widetilde{K}_s + s\widetilde{C}_s + \widetilde{K}_s)^{-1} \Phi^{\mathrm{T}}] F = H_{(s)} F \tag{18}$$

s is the Laplace variable and $H_{(s)}$ the dynamic flexibility matrix [19]. The eigenfrequencies are sorted as $\omega_1 < \omega_2 < \cdots < \omega_n$ where n is the number of considered modes of the discrete system. The flexible structure is supposed to vibrate at a frequency around a well separated mode N. This means that we suppose $\omega_N \omega_i$ if $i < N$ and $\omega_N \omega_i$ if $i > N$. H can then be written as:

$$H_{(s)} = \frac{\Phi_N \Phi_N^{\mathrm{T}}}{\mu_N (s^2 + 2\xi_N \omega_N s + \omega_N^2)} + R_N^0 \tag{19}$$

with:

$$R_N^0 = \frac{1}{s^2} \sum_{i=1}^{N-1} \frac{\Phi_i \Phi_i^{\mathrm{T}}}{\mu_i} + \sum_{i=N+1}^{n} \frac{\Phi_i \Phi_i^{\mathrm{T}}}{\mu_i \omega_i^2} \tag{20}$$

In Equation (19), the constant matrix R_N^0 is the static contribution of the low and high frequency modes of the structure [23]. If the excitation frequency ω is close enough to the natural frequency ω_N, it is possible to neglect the static residues. This assumption is made for the analytical model developed in Section 5.3, as the flexible structure is considered as a spring mass system.

DOI: 10.1002/stc

4.2. Modeling of the chosen harvesting device

Let us consider the energy harvesting device presented in Figure 5. It is composed of an electromagnetic transducer connected to an impedance $Z_f(\omega)$, which represents the resistive feedback loop [19]. It is a simplified representation of the storing system including the battery and the rectifying electronic.

The transducer is composed of a moving coil in a magnetic field created by a magnet. The relative velocity $\dot{y}_i$ (Figure 5) is imposed by the flexible structure. Equations (21) and (22) are the electromagnetic transducer's coupling laws.

$$f_i = -C_e i_i \tag{21}$$

$$\mathrm{emf}_i = C_e \frac{\mathrm{d}y_i}{\mathrm{d}t} \tag{22}$$

Variable i_i is the current flow in the transducer's coil 'i' and emf_i the electromagnetic force. The coupling coefficient C_e, which appears in Equations (21) and (22), is a constant that depends on the magnetic field, the number of turns of the coil and the length of one turn.

Here we can notice that all the mechanical power $\dot{y}_i.f_i$ is transformed into electrical power $\mathrm{emf}_i.i_i = C_e\dot{y}_i.\frac{f_i}{C_e}$. This indicates that the transducer is supposed perfect as it has an efficiency of 100%.

The harvesting device presented in Figure 5 is modeled by the passive electrical circuit shown in Figure 6. The coil's inductance L_b and its internal resistance R_b are modeled. They are added to the electromagnetic force emf_i and to the storing impedance Z_f.

The associated electrical equation gives Equation (23):

$$V_i = -(R_b + L_b s)i_i + \mathrm{emf}_i = Z_f i_i \tag{23}$$

Combining Equations (21)–(23) leads to the expression of the feedback transfer function $G_i(s)$:

$$G_i(s) = -\frac{f_i}{s\,y_i} = \frac{C_e^2}{Z_f + R_b + L_b s} \tag{24}$$

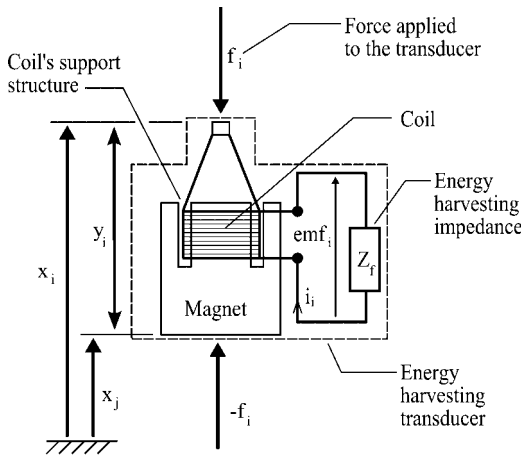

Figure 5. Structure of an energy harvesting transducer.

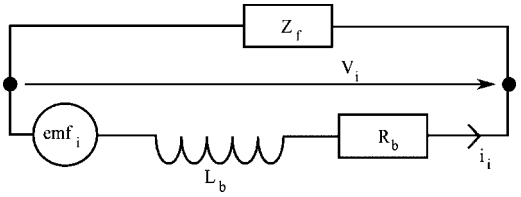

Figure 6. Passive electrical circuit.

DOI: 10.1002/stc

This equation shows that the chosen harvesting device respects the control law defined on Equation (5).

4.3. Modeling of the structure with one connected energy harvester

Now that the structure and the harvesting device are modeled, let us connect them together. Figure 7 represents the energy harvesting configuration studied. Only one harvesting device is considered. Torah *et al.* [24] have used a cantilever beam excited by an acceleration imposed to the beam's support to harvest energy. In their experiment the electromagnetic energy harvesting device is connected to the free end of the beam. In our setup, the harvesting device can be connected to any moving point of a flexible structure.

To simplify the experimental measurements, we will suppose that the external force f is imposed at only one point (point 1). This allows an easy experimental evaluation of the power provided to the flexible structure. For the rest of this study we will use the notation f_1 for the imposed force at point 1. x_1 is the displacement at point 1. f_2 represents the force vector applied by the energy harvesting device and x_2 the corresponding displacement vector.

Let us see the influence of this energy harvesting on the structure. The displacements at points 1 and 2 are defined as $x_1 = b_1^{\mathrm{T}}x$ and $x_2 = b_2^{\mathrm{T}}x$, where b_1 and b_2 are the influence vectors. We will suppose that f_1, x_1, f_2 and x_2 are real scalar functions for the rest of the study. The force vector $f = b_1 f_1 + b_2 f_2$ depends on the external shear force f_1 and the feedback shear force f_2. Let us consider the transfer functions $h_{ij} = x_i/f_j$ defined by:

$$\begin{aligned} x_1 &= h_{11} f_1 + h_{12} f_2 \\ x_2 &= h_{21} f_1 + h_{22} f_2 \end{aligned} \quad . \tag{25}$$

From Equation (19), (20) and (25) we obtain the following transfer functions h_{ij} for one mode N:

$$\begin{aligned} h_{11} &= \frac{a_{11}}{s^2 + 2\xi_N \omega_N s + \omega_N^2} + r_{11}^0 \\ h_{12} &= \frac{a_{12}}{s^2 + 2\xi_N \omega_N s + \omega_N^2} + r_{12}^0 \\ h_{21} &= h_{12} \\ h_{22} &= \frac{a_{22}}{s^2 + 2\xi_N \omega_N s + \omega_N^2} + r_{22}^0 \end{aligned} \quad . \tag{26}$$

where the coefficients $a_{ij} = b_i^{\mathrm{T}} \Phi_N \Phi_N^{\mathrm{T}} b_j / \mu_N$ and the static residues $r_{ij}^0 = b_i^{\mathrm{T}} R_N^0 b_j$ (which represent the influence of the high frequency components of the modal decomposition) have been introduced to simplify the notations.

The energy harvester connected on point 2 of the flexible structure, shown in Figure 7, implies a harvesting feedback according to Equation (24): $f_2 = -G\dot{x}_2$. Adding the feedback harvesting law to Equation (25) it is possible to deduce the Frequency Response Function

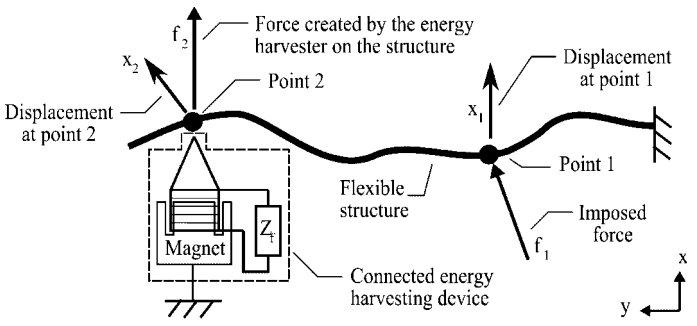

Figure 7. Modeling of the studied energy harvesting device on the support structure.

DOI: 10.1002/stc

(FRF) of the flexible structure with a feedback loop corresponding to the harvesting circuit:

$$\begin{aligned} H_1 &= \frac{x_1}{f_1} = h_{11} - sG\frac{h_{12}^2}{1+sGh_{22}} \\ H_2 &= \frac{x_2}{f_1} = \frac{h_{12}}{1+sGh_{22}} \end{aligned} \quad . \tag{27}$$

Equation (27) allows the study of the influence of the feedback loop on the FRF H_1 and H_2 with only one input f. If points 1 and 2 are collocated we have $H_1 = H_2$.

5. ENERGETIC STUDY

Stephen [25] optimizes the energy harvesting of a spring mass magnet moving through a coil. The energy scavenged by the coil is dissipated through a load resistance. This article shows that the resistance can be chosen to maximize the harvested energy from the vibrating structure. Our goal here is to precisely examine the influence of the resistance and the excitation frequency on the harvested energy. The impedance Z_f plugged onto the coil is supposed purely resistive. Let us introduce the total impedance Z_t, which corresponds to the coil's impedance (R_b+sL_b) added to the storing impedance Z_f. We then have:

$$Z_t = (Z_f+R_b)+sL_b \tag{28}$$

To simplify the notations let us introduce the real coefficients a and b, defined as:

$$\begin{aligned} a &= Z_f+R_b \\ b &= L_b \end{aligned} \quad . \tag{29}$$

5.1. Condition to harvest energy

The formulas of Equation (27) allow the calculation of the displacements x_1 and x_2 when an external force f_1 is applied to the flexible structure. f_2 is the force applied to the flexible structure by the harvesting device and here the feedback loop matrix G is a scalar defined by:

$$G = -\frac{f_2}{\dot{x}_2} = \frac{C_e^2}{a+bs} \tag{30}$$

It is then possible to evaluate the average power P_1 and P_2 respectively provided to the structure by coil 1 and harvested by the harvesting device (composed of a passive circuit connected to coil 2):

$$P_1 = \tfrac{1}{2}Re(\overline{sx_1}f_1) = \tfrac{1}{2}\|f_1\|^2 Re(sH_1) \tag{31}$$

$$P_2 = \tfrac{1}{2}Re(\overline{sx_2}f_2) = \tfrac{1}{2}\|s\|^2\|f_1\|^2\|H_2\|^2 Re(G) \tag{32}$$

To harvest energy the cost function J_h has to be positive. As $J_h = P_2$, this implies the harvesting condition on G:

$$Re(G) > 0 \tag{33}$$

5.2. Numerical study

The average powers P_1 and P_2 can be evaluated from Equations (31) and (32). Figure 8(a),(b) show their evolution for a given shear force f_1 of 1 N versus the imposed frequency and the dissipative resistance a.

Equation (32) shows that P_2 can be maximal when H_2 is maximal, which happens when the excitation frequency is close to the imaginary part of the H_2 pole. It is then interesting to examine the root locus of H_2 when the total resistance a varies. We then have to solve:

$$1+sG_{(s)}.h_{22\,(s)} = 0 \tag{34}$$

The solution s of Equation (34) is plotted for $a \in [0; +\infty[$ and gives the root locus shown in Figure 9.

DOI: 10.1002/stc

It is interesting to plot the evolution of the maximal average power for different resistances a when the frequency varies (Figure 10). This corresponds to the ridge of the surfaces of Figure 8(a), (b).

The curves in Figures 9 and 10 have some particular points of interest:

- Points A_1 and A_2 correspond to the open loop system ($a \to \infty$), power P_2 is then equal to zero.
- Points E_1 and E_2 correspond to the closed loop system ($a = 0$), power P_2 is equal to zero. Physically, this system is equivalent to a beam with the displacement stiffened by the coil at point 2.
- Point C is where the system is the most damped. In this case, the yield is very high (close to 100%). However, as the system is very damped, the input power is very low.
- Points B_1, B_2, D_1, D_2 correspond to maximums of dissipated power P_2. In this case the energy harvested is optimized.

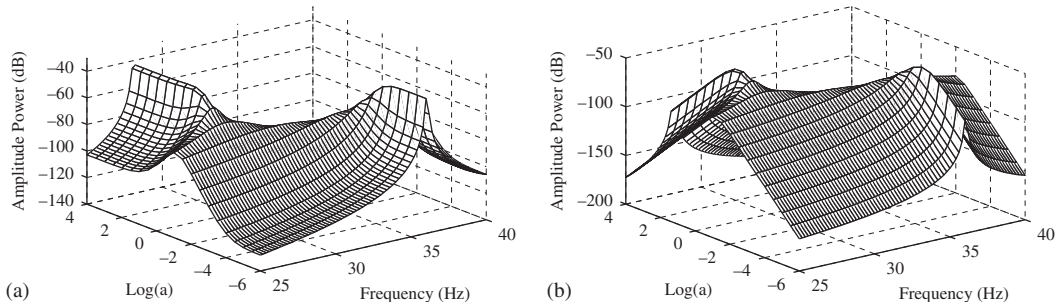

Figure 8. Power versus the frequency and the resistance a: (a) P_1 and (b) P_2.

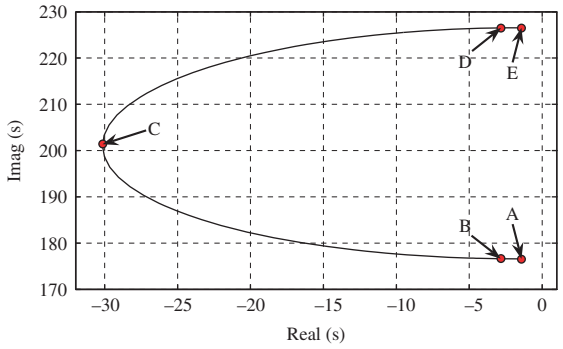

Figure 9. Root locus of H_2 when the total resistance a varies.

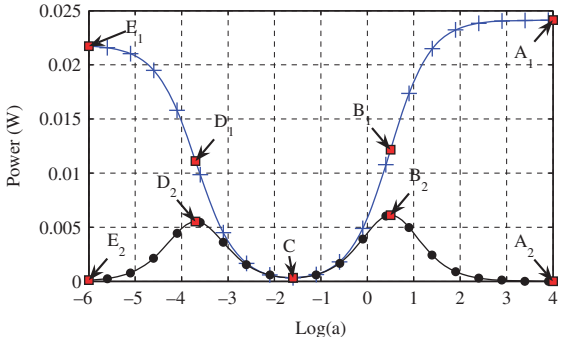

Figure 10. Powers $P_1(+)$ and $P_2(\bullet)$ versus the total resistance a when the frequency maximizes P_2.

DOI: 10.1002/stc

These results show that for an external sinusoidal force f_1 with a constant amplitude around the first bending mode, it is possible to find two maximums: one for a 'low' resistance and one for a 'high' resistance. The 'high' resistance is found in Stephen's article [25], but the 'low' one is not.

If we had just considered the energy harvester as a simple damper, we would not have obtained the second maximal power harvested (node D_2) in Figure 10.

5.3. Analytical study

To be able to develop an analytical solution, a two-input two-output system is created and the static residues are neglected. r_{11}^0, r_{12}^0, r_{22}^0 are then equal to zero, and Equation (26) gives a formulation that is equivalent to a spring mass system. By noting that $a_{11} \times a_{22} = a_{12}^2$, as $\Phi_N^{\mathrm{T}} b_1$ and $\Phi_N^{\mathrm{T}} b_2$ are scalars, it is possible to write the power P_1 and P_2 versus the transfer functions h_{22} and G:

$$\begin{aligned} P_1 &= \frac{1}{2}\|f_1\|^2 \frac{a_{11}}{a_{22}} Re\left(s\left[\frac{h_{22}}{1+Gh_{22}}\right]\right) \\ P_2 &= \frac{1}{2}\|f_1\|^2 \frac{a_{11}}{a_{22}} \left\|\frac{h_{22}}{1+Gh_{22}}\right\|^2 Re(\bar{s}G) \end{aligned} \tag{35}$$

As $s = \mathrm{j}\omega$, we have $Z_t = a + \mathrm{j}\omega b$. Hence the power expressions P_1, P_2 and the efficiency η can be written as Equations (36)–(38).

$$P_1 = \frac{\frac{1}{2}\|f_1\|^2 a_{11}\omega^2(2\xi_N\omega_N[a^2+(b\omega)^2]+C_e^2 a_{22}a)}{[a(\omega_N^2-\omega^2)-2\xi_N\omega_N b\omega^2]^2+[C_e^2 a_{22}+b(\omega_N^2-\omega^2)+2\xi_N\omega_N a]^2\omega^2} \tag{36}$$

$$P_2 = \frac{\frac{1}{2}\|f_1\|^2 C_e^2 a_{12}^2 a\omega^2}{[a(\omega_N^2-\omega^2)-2\xi_N\omega_N b\omega^2]^2+[C_e^2 a_{22}+b(\omega_N^2-\omega^2)+2\xi_N\omega_N a]^2\omega^2} \tag{37}$$

$$\eta = \frac{P_2}{P_1} = \frac{C_e^2 a_{22} a}{2\xi_N\omega_N[a^2+(b\omega)^2]+C_e^2 a_{12}a} \tag{38}$$

These expressions allow an analytical resolution of the special points shown in Figure 10.

The notation ω_{N_E} is the eigenfrequency of the beam blocked on point 2 (points E_1 and E_2):

$$\omega_{N_E} = \sqrt{\omega_N^2 + \frac{C_e^2 a_{22}}{b}} \tag{39}$$

The goal is to compare the points (A to E) on the root locus Figure 9 and the maximal power in Figure 10. Therefore, it is necessary to find the poles of Equation (34). They are the solutions of:

$$(a+bs)(s^2+2\xi_N\omega_N s+\omega_N^2)+C_e^2 a_{22}s = 0 \tag{40}$$

5.3.1. Point E. In the case $a = 0$, the solution of Equation (40) is

$$s = -\xi_N\omega_N \pm \mathrm{j}\sqrt{\omega_{N_E}^2 - \omega_N^2\xi_N^2} \approx -\xi_N\omega_N \pm \mathrm{j}\omega_{N_E} \tag{41}$$

The expression of P_1 in Equation (36) becomes:

$$P_1 = \frac{1}{2}\|f_1\|^2 \frac{a_{11}2\xi_N\omega_N}{(2\xi_N\omega_N)^2+\left[\left(\frac{\omega_{N_E}}{\omega}\right)^2-1\right]^2} \tag{42}$$

DOI: 10.1002/stc

The maximum of the function $P_{1\,(\omega)}$ is found when $\omega = \omega_{N_E}$. Hence from Equations (36) to (38) we obtain the expressions of P_1, P_2, and η:

$$\begin{aligned} P_1 &= \frac{a_{11}\,\|f_1\|^2}{4\xi_N\omega_N} \\ P_2 &= 0 \\ \eta &= 0 \end{aligned} \tag{43}$$

5.3.2. Point D. Here $a \ll b\|s\|$. Consequently, $\omega_{N_E}^2 \gg 2\xi_N\omega_N\frac{a}{b}$ as $\omega_{N_E} > 2\xi_N\omega_N$. Then Equation (40) can be simplified:

$$s^3 + \left(2\xi_N\omega_N + \frac{a}{b}\right)s^2 + \omega_{N_E}^2 s + \frac{a\omega_N^2}{b} = 0 \tag{44}$$

Since the solution of Equation (44) is $s = -\xi\omega + \mathrm{j}\omega$ then $s^2 \approx -\omega^2 2\mathrm{j}\xi\omega^2$ and $s^3 \approx 3\xi\omega^3 - \mathrm{j}\omega^3$ as $\xi \ll 1$. Using s, s^2 and s^3 expressions and taking the imaginary part of the solution s of Equation (44), it is possible to show that $\omega \approx \omega_{N_E}$. Taking the real part of Equation (44) leads to:

$$\xi\omega = \xi\omega_{N_E} = \frac{\omega_{N_E}^2 - \omega_N^2}{2\omega_{N_E}^2}\frac{a}{b} + \xi_{N_E}\omega_{N_E} \tag{45}$$

At the node D, a maximizes the function $P_{2\,(a)}$. Taking the expression of P_2 in Equation (37) and solving $(\partial P_2/\partial a) = 0$ gives the optimal value of a for each frequency ω:

$$a = b\omega\sqrt{\frac{(2\xi_N\omega_N)^2\omega^2 + (\omega_{N_E}^2 - \omega^2)^2}{(\omega_N^2 - \omega^2)^2 + (2\xi_N\omega_N\omega)^2}} \tag{46}$$

After developing Equation (37) and neglecting some terms as $\xi_N \ll 1$ and $a \ll b\omega$, it is possible to show that when $\omega \approx \omega_{N_E}$ the power P_2 is maximized. Using Equation (46), we obtain:

$$a \approx b\frac{2\xi_N\omega_N\omega_{N_E}^2}{\omega_{N_E}^2 - \omega_N^2} = \frac{2\xi_N\omega_N}{C_e^2 a_{22}}(b\omega_{N_E})^2 \tag{47}$$

It is then possible to write the solution of Equation (44): $s \approx -2\xi_N\omega_N \pm \mathrm{j}\omega_{N_E}$. When $\omega = \omega_{N_E}$, the function $P_{2\,(\omega)}$ is maximum. Hence from Equations (36) to (38) we obtain the expressions of P_1, P_2 and η:

$$\begin{aligned} P_1 &= \frac{a_{11}\|f_1\|^2}{8\xi_N\omega_N} \\ P_2 &= \frac{a_{11}\|f_1\|^2}{16\xi_N\omega_N}. \\ \eta &= \frac{1}{2} \end{aligned} \tag{48}$$

5.3.3. Point C. In this case the function $P_{2\,(a)}$ is minimum and the yield $\eta_{(a)}$ has to be maximum because the damping of the structure is maximized and the loss is minimized. The yield function is maximum when $a = b\omega$. At this point the minimum power P_2 is obtained when $(\partial P_2/\partial a) = 0$

DOI: 10.1002/stc

and leads to Equation (46). Those two conditions on a give:

$$\omega = \omega_{N_C} = \sqrt{\frac{\omega_{N_E}^2 + \omega_N^2}{2}} \tag{49}$$

If we suppose that $\frac{\omega_{N_E} - \omega_N}{\omega_N} \ll 1$, then:

$$\omega_{N_C} \approx \frac{\omega_{N_E} + \omega_N}{2} \tag{50}$$

Equation (40) of the root locus can be simplified using the condition $\frac{a}{b} = \omega_{N_C}$:

$$s^3 + (2\xi_N\omega_N + \omega_{N_C})s^2 + (2\xi_N\omega_N\omega_{N_C} + \omega_{N_E}^2)s + \omega_{N_C}\omega_N^2 = 0 \tag{51}$$

We use the notation $s = -\xi\omega_{N_C} + j\omega_{N_C}$ and the approximated expressions of s^2 and s^3 like for the study of 'Point D.' If we only keep the real part, we obtain:

$$(\xi\omega)_{N_C} = \left(\frac{\omega_{N_E}^2 - \omega_N^2}{3\omega_N^2 + \omega_{N_E}^2}\right)\omega_{N_C} \tag{52}$$

When $\omega = \omega_{N_C}$, Equation (36)–(38) give the expressions of P_1, P_2 and η:

$$\begin{aligned} P_1 &= \| f_1 \|^2 a_{11} \frac{\dfrac{b\omega_{N_C}}{C_e^2 a_{22}}}{\left[1 - 2\xi_N\omega_N \dfrac{2b\omega_{N_C}}{C_e^2 a_{22}}\right]} \\ P_2 &= \| f_1 \|^2 a_{11} \frac{\dfrac{b\omega_{N_C}}{C_e^2 a_{22}}}{\left[1 - 2\xi_N\omega_N \dfrac{2b\omega_{N_C}}{C_e^2 a_{22}}\right]^2} \\ \eta &= 1 - 2\xi_N\omega_N \frac{2b\omega_{N_C}}{C_e^2 a_{22}} \end{aligned} \tag{53}$$

5.3.4. Point B. Here $a \gg b\|s\|$. Then Equation (40) can be simplified by:

$$a(s^2 + 2\xi_N\omega_N s + \omega_N^2) + C_e^2 a_{22} s = 0 \tag{54}$$

The solution of this equation is:

$$s = -\xi_N\omega_1 - \frac{C_e^2 a_{22}}{2a} \pm j\omega_N\sqrt{1 - \xi_N^2\left(+\frac{C_e^2 a_{22}}{2\xi_N\omega_N a}\right)^2} \tag{55}$$

To get the resistance a and the frequency ω, which maximize P_2, we are using the same technique as the one used to find the parameters for 'Point D' Neglecting $\xi_N \ll 1$ and $a \gg b\omega$ allow us to prove that $P_{2\,(\omega)}$ is maximized when $\omega = \omega_N$ and:

$$a = \sqrt{(b\omega_N)^2 + \left(\frac{C_e^2 a_{22}}{2\xi_N\omega_N}\right)^2} \tag{56}$$

With the hypothesis $a \gg b\omega$ and the expression of a in Equation (56), we get $C_e^2 a_{22}/2\xi_N\omega_N \gg b\omega_N$ and thus:

$$a \approx \frac{C_e^2 a_{22}}{2\xi_N\omega_N} \tag{57}$$

DOI: 10.1002/stc

The solution of Equation (55) can be simplified: $s \approx -2\xi_N\omega_N \pm j\omega_N$. Hence from Equations (36) to (38) we obtain the expressions of P_1, P_2, and η:

$$\begin{aligned} P_1 &= \frac{a_{11}\|f_1\|^2}{8\xi_N\omega_N} \\ P_2 &= \frac{a_{11}\|f_1\|^2}{16\xi_N\omega_N} \\ \eta &= \frac{1}{2} \end{aligned} \tag{58}$$

5.3.5. Point A. In the case $a \to \infty$ Equation (40) can be divided by a. Hence the equation to solve is:

$$s^2+2\xi_N\omega_N s+\omega_N^2 = 0 \tag{59}$$

The solution of this equation is:

$$s = -\xi_N\omega_N \pm j\omega_N\sqrt{1-\xi_N^2} \approx -\xi_N\omega_N \pm j\omega_N \tag{60}$$

The expression (36) of the power P_1 with the condition $a \gg b\omega$ is:

$$P_1 = \frac{1}{2}\left\{\frac{\|f_1\|^2 a_{11}\omega^2 2\xi_N\omega_N a^2}{a^2(\omega_N^2-\omega^2)^2+\omega^2(2\xi_N\omega_N)^2a^2}\right\} \tag{61}$$

The maximum of the function $P_{1\,(\omega)}$ is found when $\omega = \omega_1$. Hence from Equations (36) to (38) we obtain the expressions of P_1, P_2 and η:

$$\begin{aligned} P_1 &= \frac{a_{11}\|f_1\|^2}{4\xi_N\omega_N} \\ P_2 &= 0 \\ \eta &= 0 \end{aligned} \tag{62}$$

5.3.6. Synthesis. The average power harvested by coil 2 is completely dissipated in the passive feedback loop. The inductance b does not dissipate any power, only the total resistance a does. The analytical powers P_1 and P_2 depend on the parameters a (resistance) and ω (excitation frequency). Looking for the frequency ω which maximizes P_2 for a resistance a leads to a graph similar to Figure 10. The analytical expression of the points of special interest (which appear on Figure 10) are given in Table I with: $\omega_{N_E} = \sqrt{\omega_N^2+C_e^2a_{22}/b}$ and $\omega_{N_C} = \left(\omega_{N_E}+\omega_N\right)/2$.

Points A and E are not interesting for energy harvesting as there is no energy transfer when $a = 0$ or $a \to \infty$. In the case $a = 0$, a feedback effect exists on the structure and changes its impedance. This explains why for a considered mode N, the natural frequency is different for a short circuit than for an open loop.

The two resistances, which maximize the harvested power P_2, are located at points B and D where P_2 is equal to half of P_1. Here the electrical damping is equal to the mechanical damping, which has already been reported for a spring mass magnet moving through a coil with a resistive load [25]. This corresponds to Jacobi's theorem. To maximize the electrical power transfer to an electrical load, the impedance has to be matched to the conjugated generator impedance. Here,

Table I. Synthesis of the analytical results for the particular points.

Point	Pole's real part (root locus)	Pole's imaginary part (root locus)	Energetic yield
A	$-\xi_N\omega_N$	ω_N	0
B	$\frac{\omega_N^2-\omega_{N_E}^2}{3\omega_N^2+\omega_{N_E}^2}2\xi_N\omega_N$	ω_N	$\frac{1}{2}$
C	$\frac{\omega_N^2-\omega_{N_E}^2}{3\omega_N^2+\omega_{N_E}^2}\omega_{N_C}$	ω_{N_C}	$1-2\xi_N\omega_N\frac{2b\omega_{N_C}}{C_e^2a_{22}}$
D	$-2\xi_N\omega_N$	ω_{N_E}	$\frac{1}{2}$
E	$-\xi_N\omega_N$	ω_{N_E}	0

DOI: 10.1002/stc

Jacobi's maximum power transfer theorem has then to be adapted to a multi-physic problem. Points B and D can be placed on the root locus (Figure 9) if we consider a direct velocity feedback at the abscissa $-2\xi_N\omega_N$. This corresponds to twice the abscissa of the structure for a short circuit ($a = 0$) or for an open circuit ($a \to \infty$). This is a consequence of the fact that P_2 is maximized when the electrical damping is equal to the mechanical one.

The resistance a at point C maximizes the damping of the structure. This corresponds to the optimal damping effect described by Monnier *et al.* [18]. This case is not interesting for energy harvesting if we consider a finite power source as the high damping leads to very small displacements of the structure.

As points B, C and D are distinct, the stabilization and harvesting strategies are then distinct in the case of an imposed external force. The maximal average power P_2 value depends neither on the electromechanical coupling coefficient C_e nor on the position of the harvesting device on the beam. Hence, there is no need to have a high magnetic field or to have the coil placed at the free end of the cantilever beam to dissipate a lot of energy in a resistance. Equations (47) and (57) show that the coupling parameter has to be known to choose the two optimal resistances a. The inverse mass parameter a_{22} depends on the position of coil 2 on the beam. Hence, the two optimal resistances have to be adjusted versus the position of the energy harvester.

6. EXPERIMENTAL VALIDATION

The goal of this experimentation is to validate the energy harvesting model developed. The experimental setup has to correspond to the model proposed in Figure 7. On this beam we can evaluate easily the provided and harvested power (collocated force and velocity measurement).

6.1. The flexible structure

The flexible structure is composed of a cantilever beam on which two electromagnetic actuators are fixed (Figure 11). Fixing one side of the electromagnetic transducer on the structure's support makes it easier to evaluate the harvested or provided power. Just one velocity and force measurement will be needed to evaluate the harvested power. The power is provided by the electromagnetic transducer 'coil 1', which appears in Figure 11. The 'coil 2', connected to an electrical impedance, is used to harvest energy. This schematic representation corresponds to the photo of the experimental setup shown in Figure 12. The beam ($525 \times 50 \times 9.6$ mm) is made of steel and studied around the first bending mode.

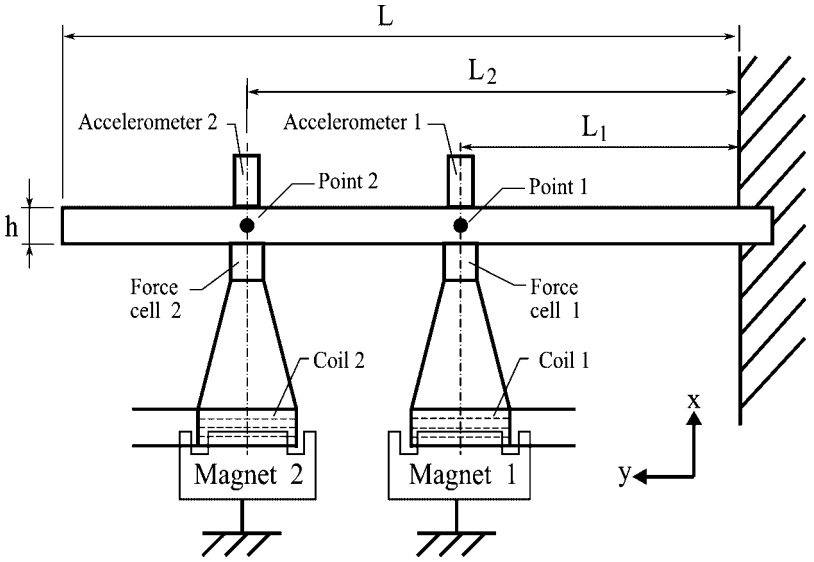

Figure 11. Schematic experimental setup.

DOI: 10.1002/stc

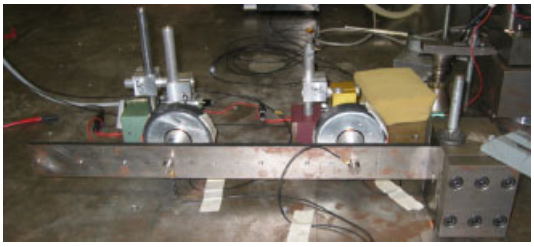

Figure 12. Experimental setup.

6.2. Actuators

The two actuators are placed respectively at distances $L_1 = 155$ mm and $L_2 = 335$ mm from the strongly fixed end (Figure 11). These 'homemade', contact-less electromagnetic actuators are constituted of a coil fixed on the structure by a cone and placed in the air-gap of a permanent magnet fixed on the ground. Both actuators have the same characteristics. The cones are designed to move the magnet away from the structure in order to decrease the direct magnetic effect on the structure. They are made of aluminum to increase the stiffness-to-mass ratio and to avoid magnetic conductivity. Together a coil and a cone weigh 14.3 g. Measurements show that the power lost when the energy is converted can be neglected.

When the transducer 'j' has a small x-axis displacement x_j (Figure 11), the coupling laws given by Equations (21) and (22) are verified. Variable f_j is the shear force induced by the electromagnetic feedback, while i_j is the current flow into the coil 'j' and emf_j the electromagnetic force. The coupling coefficient's value $C_e = 2.1\ \text{N.A}^{-1}$ is identified by experiment. Both coils have an internal resistance of $R_b = 0.70\ \Omega$, and an inductance of $L_b = 70\ \mu\text{H}$.

Coil 1 is used to excite the structure by imposing an external sinusoidal force f_1 with a constant amplitude at a given frequency ω(chosen close to the frequency of the first bending mode). Coil 2 is used to harvest the vibrating energy from the structure and to dissipate the converted electrical power in a resistive feedback load impedance Z_f.

6.3. Instrumentation

A force cell is placed between the coil and the structure to measure the effort produced by each actuator. Accelerometers are collocated with the force cells, but are placed on the other side of the beam (Figure 11). These sensors permit the evaluation of the provided and harvested mechanical power by the transducers. The energy harvested is dissipated in the storing impedance Z_f connected to coil 2. The measures of Z_f and of the current flow i_2 give the electrical power dissipated and is compared to the energy harvested. The storing impedance Z_f is obtained by an ohmmeter. The electrical current is measured by a Hall effect probe. The Hall effect probe is chosen to not disturb the harvesting circuit as the current flow is low.

6.4. Modeling of the experimental setup

The cantilever beam is discretized by Euler-Bernoulli elements such that some points coincide with the positions of the two actuators. Let us call them point 1 and point 2 as shown in Figure 7. The accelerometers and the force cells are modeled by lumped masses on points 1 and 2. x_1, f_1 and x_2, f_2 represent the displacement and the shear force applied at point 1 and point 2. The theoretical Young's modulus of the steel beam has been lightly modified in order to minimize the error between the numerical first bending frequency and the one measured experimentally (Table II).

On the experimental setup the natural frequencies without feedback loop have been measured. Table II shows that all the modes are separated and that the structure is slightly damped ($\xi_i \ll 1$). Here N is chosen equal to 1.

We can see that the comparison of numerical FRF at point 1 with 1 mode and 6 modes are well superimposed on the frequency band [25 Hz; 40 Hz] as shown in Figure 13. The assumption of modeling the flexible structure by a one degree of freedom system is validated. The

DOI: 10.1002/stc

comparison between experimental and numerical results in Figure 13 shows that the curves are well superimposed too. This confirms that the chosen beam model is valid for the natural frequencies considered. We can then use the system defined in Equation (26).

6.5. *Prediction from the numerical and analytical model*

The energetic models developed in Section 5.2 are applied to the experimental setup. Table III shows the numerical and analytical results for points B, C and D. Despite the fact that the modeling of the structure has been simplified to obtain analytical results, it can be noted that there is a good agreement between the resistances a and the energetic yield η at the special points. The assumption of neglecting the static residues r_{ij}^0 in Equation (26) is then valid.

It will not be possible to observe experimentally the maximum power P_2 of point D for a purely resistive feedback as the resistance $a = 2 \times 10^{-4}\ \Omega$ at this point is below the coil's internal resistance $R_b = 0.7\ \Omega$. Equation (47) shows that it might be possible to reach this point by adding a high inductance with a low internal resistance to the feedback loop. Therefore, the only storing impedance $Z_{f\,\mathrm{opt}}$ to plug onto the coil which optimizes the average power P_2 is:

$$Z_{f\,\mathrm{opt}} = \frac{a_{22} C_e^2}{2\xi_N \omega_N} - R_b \tag{63}$$

$Z_{f\,\mathrm{opt}}$ depends on: the electromechanical coupling coefficient C_e, the coil's resistance R_b and the structure's damping ratio ξ_N.

Table II. Experimental and numerical results for the open loop beam.

	Mode 1	Mode 2	Mode 3	Mode 4
Experimental natural frequency (Hz)	28.09	174.2	478.7	942
Experimental damping ratio ξ_i (%)	0.205	0.195	0.098	0.158
Numerical natural frequency (Hz)	28.11	174.1	477.6	970.6

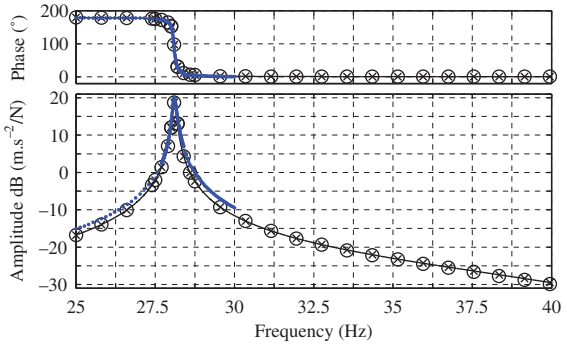

Figure 13. FRF h_{11}, open loop beam: experimental (•), simulated with 1 mode (×), simulated with 6 modes (○).

Table III. Comparison of the analytical and numerical results.

	Resistance $a(\Omega)$			Energetic yield η		
	Numeric	Analytic	Error	Numeric	Analytic	Error
B	3.16	3.17	0.32%	0.5025	0.5	0.5%
C	2.51×10^{-2}	2.22×10^{-2}	11.5%	0.9858	0.9860	0.02%
D	2.00×10^{-4}	1.97×10^{-4}	1.5%	0.4959	0.5	0.82%

DOI: 10.1002/stc

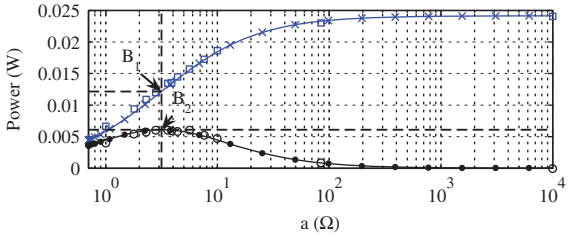

Figure 14. Maximal power in the actuators versus total feedback resistance: P_1 simulated (×); P_2 simulated (●); P_1 measured (□); P_2 measured (○).

6.6. Experimental energy harvesting results

The experimental flexible structure is excited by an external sinusoidal shear force f_1 with a constant amplitude of 1 N. The frequency ω is chosen around the first bending mode to maximize the power P_2 dissipated in the resistance a. The optimal frequency is experimentally found at $\omega = \omega_1 = 178\ \text{rad.s}^{-1}$. Only the resistances higher than the coil's internal resistance $R_b = 0.7\ \Omega$ are tested during the experimental measurements.

The accelerometer 1 and cell force 1 (Figure 11) are used to evaluate the value of the provided average power P_1, thanks to the equation:

$$P_1 = P_{1_m} = \frac{1}{\frac{2\pi}{\omega}} \int_0^{2\pi/\omega} f_1 \left(\frac{\mathrm{d}x_1}{\mathrm{d}t}\right) \mathrm{d}t \tag{64}$$

where P_{1_m} is the mechanical average power at point 1.

To evaluate the average power P_2 at point 2, it was decided not to use the mechanical average power P_{2_m}, as it is not possible to get a precise value of the applied force f_2. When the beam is at its first bending mode the force cell 2 is strongly perturbed by an inertial force. By using Equations (21) and (22), it is possible to show that the average electrical power P_{2_e} is equal to P_{2_m} at point 2.

$$P_{2_m} = \frac{1}{\frac{2\pi}{\omega}} \int_0^{2\pi/\omega} f_2 \left(\frac{\mathrm{d}x_2}{\mathrm{d}t}\right) \mathrm{d}t = \frac{1}{\frac{2\pi}{\omega}} \int_0^{\frac{2\pi}{\omega}} (C_e i_2).\left(\frac{V_2}{C_e}\right) \mathrm{d}t = P_{2_e} \tag{65}$$

The electrical power (P_{2_e}) dissipated in the electrical circuit is obtained by using the equation:

$$P_{2_e} = \frac{1}{\frac{2\pi}{\omega}} \int_0^{2\pi/\omega} V_2.i_2\,\mathrm{d}t = \frac{1}{2}\,a(i_{2_{\text{eff}}})^2 \tag{66}$$

where a is the total resistance of the circuit and $i_{2_{\text{eff}}}$ the effective current in the coil 2. A Hall effect probe gives the current (i_2) and an ohmmeter the value of resistance Z_f plugged onto the coil 2 (Figure 6). The value of the total resistance $a = R_b + Z_f$ and the value of P_{2_e} can then easily be deduced.

The experimental powers P_1 and P_2 are compared to numerical simulations for different values of $a \geqslant R_b$. The average error on P_1 is 6% and on P_2 is 12%. Figure 14 shows a very good agreement between the numerical simulations and the experimental measurements. The experiment confirms that there is a maximum of power P_2 dissipated around the functioning point D where $a = 3.16\ \Omega$ and the yield $\eta = \frac{1}{2}$.

7. CONCLUSION

The present study focuses on optimizing the harvested energy from a flexible structure. The harvesting device is composed of an electromechanical transducer connected to an impedance which models the storing electronic. This device is fixed on a flexible structure and creates a

DOI: 10.1002/stc

viscous feedback G on it. This situation is analogous to the case of a classical Direct Velocity Feedback control.

An analytical model of a flexible structure with a single energy harvester has been developed. This model enlarges the results given in the case of a spring mass model [25] to a flexible structure around an isolated mode. It also shows that the maximum dissipated power with an external electromagnetic energy harvesting device depends neither on the coupling coefficient nor on the position on the structure as long as the harvesting connected point is moving. It only depends on the structure's damping ratio if the excitation frequency coincides with that of the optimal functioning point. This implies that it is not necessary to have a high magnetic field or to place the coil at the free end of a cantilever beam to maximize the harvested energy. However, the impedance plugged onto the coil has to be adjusted versus the coupling coefficient and the position of the transducer on the flexible structure.

The maximal power is extracted when the electrical and mechanical damping ratios are equal. This result is valid if the structure is excited at an isolated frequency and submitted to an imposed acceleration or an imposed force. This corresponds to applying Jacobi's theorem to a multi-physic problem. In Stephen's article [25] only one resistance matching the electrical and mechanical damping ratios is presented. In our study a second resistance matching the damping ratios has been obtained as the coil's inductance (used by the electromechanical transducer) has been added to the modeling. The analytical spring mass model, derived from the flexible structure, confirms that both optimal energy harvesting resistances are obtained for matching damping ratios. Analytical energy transfer expressions give optimal design parameters when a linear device is plugged on the electromagnetic transducer. They show that for both optimal resistances half of the provided energy can be harvested. On the root locus, the two optimal energy harvesting feedback gains have the same abscissa, which is equal to twice the no energy transfer abscissa (open circuit or short circuit). The root locus can then be used to choose the optimal energy transfer gain in the case of a DVF law control for an imposed excitation force or acceleration.

The experimental measurements are in good agreement with numerical simulations, and confirm that it is possible to maximize the average power dissipated in a purely resistive impedance plugged onto a coil. The value of the optimal 'high' resistance is close to those predicted by the analytical expression and obtained by numerical simulations. The 'low' resistance could not be reached experimentally as the optimal resistance is below the transducer's coil internal resistance. A possible way to overcome this limitation would consist in having a storing resistance with a 'high' value of inductance.

The analytical results are very useful for choosing the resistance, which maximizes the dissipated energy while designing a vibrating energy harvesting system. The results obtained are applicable for macro- and micro-scale electromagnetic generators as shown by Beeby *et al*. [26]. Future studies will involve optimizing vibrating energy harvesting using a non-linear feedback loop [27].

REFERENCES

1. Leijon M, Danielsson O, Eriksson M, Thorburn K, Bernhoff H, Isberg J, Sundberg J, Ivanova I, Sjöstedt E, Ågren O. An electrical approach to wave energy conversion. *Renewable Energy* 2006; **31**:1309–1319.
2. Casciati F, Rossi R. A power harvester for wireless sensing applications. *Structural Control and Health Monitoring* 2007; **14**(4):649–659.
3. Cui Y, Gao RX, Yang D, Kazmer DO. A bond graph approach to energy efficiency analysis of a self-powered wireless pressure sensor. *Smart Structures and Systems* 2007; **3**(1):1–22.
4. James EP, Tudor MJ, Beeby SP, Harris NR, Glynne-Jones P, Ross JN, White NM. An investigation of self-powered systems for condition monitoring applications. *Sensors and Actuators A* 2004; **110**:171–176.
5. Farra CR, Park G, Allen DW, Todd MD. Sensor network paradigms for structural health monitoring. *Structural Control and Health Monitoring* 2006; **13**(1):210–225.
6. Nagayama T, Spencer Jr BF, Rice JA. Autonomous decentralized structural health monitoring using smart sensors. *Structural Control and Health Monitoring* 2009; **16**:842–859.
7. Lefeuvre E, Badel A, Richard C, Petit L, Guyomar D. A comparison between several vibration-powered piezoelectric generators for standalone systems. *Sensors and Actuators A* 2006; **126**:405–416.
8. Cavallier B, Berthelot P, Nouira H, Foltête E, Hirsinger E, Ballandras S. Energy harvesting using vibrating structures excited by shock, *IEEE International Ultrasonics Symposium*, Rotterdam, The Netherlands, 2005.

DOI: 10.1002/stc

9. Tiwari R, Kim KJ, Kim S-M. Ionic polymer-metal composite as energy harvesters. *Smart Structures and Systems* 2008; **4**(5):549–563.
10. Mitcheson PD, Miao P, Stark BH, Yeatman EM, Holmes AS, Green TC. MEMS electrostatic micropower generator for low frequency operation. *Sensors and Actuators A* 2004; **115**:523–529.
11. Glynne-Jones P, Tudor MJ, Beeby SP, White NM. An electromagnetic, vibration-powered generator for intelligent sensor system. *Sensors and Actuators A* 2004; **110**:344–349.
12. El-hami M, Glynne-Jones P, white NM, Hill M, Beeby S, James E, Brown AD, Ross JN. Design and fabrication of a new vibration-based electromechanical power generator. *Sensors and Actuators A* 2001; **92**:335–342.
13. Mitcheson PD, Green TC, Yeatman EM, Holmes AS. Architectures for vibration-driven micropower generators. *Journal of Microelectromechanical Systems* 2004; **13**(3):429–440.
14. von Büren T, Mitcheson PD, Green TC, Yeatman EM, Holmes AS, Tröster G. Optimization of inertial micropower generators for human walking motion. *IEEE Sensors Journal* 2006; **6**(1):28–38.
15. Sterken T, Baert K, Van Hoof C, Puers R, Borghs G, Fiorini P. Comparative modelling for vibration scavengers [MEMS energy scavengers], Sensors, *Proceedings of IEEE*, vol. 3, 24–27 October 2004; 1249–1252.
16. Lesieutre GA, Ottman GK, Hofmann HF. Damping as a result of piezoelectric energy harvesting. *Journal of Sound and Vibration* 2004; **269**:991–1001.
17. Williams CB, Yates RB. Analysis of a micro-electric generator for Microsystems. *Sensors and Actuators A* 1996; **52**:8–11.
18. Monnier P, Collet M. Definition of the mechanical design parameters to optimize efficiency of integral force feedback active damping strategy. *Journal of Structural Control* 2005; **12**:65–89.
19. Preumont A. *Vibration Control of Active Structures*: *An Introduction* (2nd edn). Kluwer: Dordrecht, 2002.
20. Tisseur F, Meerbergen K. The quadratic eigenvalue problem. *SIAM Review* 2001; **43**(2):235–286.
21. Komornik V. Rapid boundary stabilization of linear distributed systems. *SIAM Journal on Control and Optimization* 1997; **35**(5):1591–1613.
22. Meyer Y, Collet M, Delobelle P. Optimisation structurale de problèmes d'amortissement actif collocalisés de type Direct Velocity Feedback. *Proceedings of 7th National Conference on Computational Structural Mechanics*, Giens, 2005.
23. Geradin M, Rixen D. *Mechanical Vibration*: *Theory and Application to Structural Dynamics*. Wiley: Chichester, 1997.
24. Torah RN, Beeby SP, Tudor MJ, O'Donnell T, Roy S. Development of a cantilever beam generator employing vibration energy harvesting. *Proceedings of the 6th International Workshop on Micro and Nanotechnology for Power Generation and Energy Conversion Applications* (*PowerMEMS 2006*), Berkeley, U.S.A., 29 November–1 December 2006; 181–184.
25. Stephen NG. On energy harvesting from ambient vibration. *Journal of Sound and Vibration* 2006; **293**:409–425.
26. Beeby SP, Tudor MJ, Koukharenko E, Roberts S, O'Donnell T, Roy S. Macro and micro scale electromagnetic kinetic energy harvesting generators, *Proceedings of DTIP Conference*, Stresa, Italy, 2006.
27. Peano F, Coppa G, Serazio C, Peinetti F, D'angola A. Nonlinear oscillations in a MEMS energy scavenger. *Mathematical and Computer Modelling* 2006; **43**:1412–1423.

DOI: 10.1002/stc